World Academy of Science, Engineering and Technology
International Journal of Physical and Mathematical Sciences
Vol:17, No:7, 2023

Mode-Locked Fiber Laser Using Charcoal and Graphene Saturable Absorbers to Generate 20-GHz and 50-GHz Pulse Trains, Respectively

Ashiq Rahman, Sunil Thapa, Shunyao Fan, Niloy K. Dutta

***Abstract*—**A 20-GHz and a 50-GHz pulse train are generated using a fiber ring laser setup that incorporates rational harmonic mode-locking (RHML). Two separate experiments were carried out using charcoal nanoparticles and graphene nanoparticles acting as saturable absorbers to reduce the pulse width generated from RHML. Autocorrelator trace shows that the pulse width is reduced from 5.6 ps to 3.2 ps using charcoal at 20 GHz, and to 2.7 ps using graphene at 50-GHz repetition rates, which agrees with the simulation findings. Numerical simulations have been carried out to study the effect of varying the linear and nonlinear absorbance parameters of both absorbers on output pulse widths. Experiments closely agree with the simulations.

***Keywords*—**Fiber optics, fiber lasers, mode locking, saturable absorbers.

I. Introduction

WORLD-wide-web and intercontinental long-distance fiber-optic communications have benefited greatly due to the improvement in high-speed transmission fibers. Fiber-optic transmission over a 40 km distance at a data rate as high as 178 Tbps has been achieved by novel fiber optic design [1]. To optically transmit data at such high rates with minimal bit-error rate, the pulses must be very narrow, and the pulse trains must have very high frequencies [2]-[4]. Several procedures have been demonstrated to generate high frequency, narrow width pulses over the years. The procedure to achieve this using a combination of active and passive mode-locking, also known as hybrid mode locking, was described in [5]. Zhang et al. used a combination of RHML and nonlinear polarization rotation to generate 30-GHz pulse trains with pulse-widths as narrow as 1.9 ps [6]. Graphene has been used as saturable absorbers in many different fiber laser designs in, including but not limited to, fiber laser [7]-[15]. Chemical vapor deposition (CVD) was used to create layers of graphene/poly methyl methacrylate (PMMA) saturable absorber in a Thulium-doped mode-locked fiber laser [16]. Similarly, a mode-locked fiber laser with tunable output power was also demonstrated by Sheng et al. [17]. Other than CVD, a viable method to obtain graphene or charcoal to be used for saturable absorption purposes is trituration, which is used in this work. Triturating various carbon-based materials, and using them for pulse shaping purposes in Erbium-doped fiber lasers, was also demonstrated by Lin et al. in [18].

This paper presents the combined incorporation of RHML and carbon-based saturable absorbers in the fiber ring laser system. Using charcoal nanoparticles in the ring laser cavity resulted in a stable output 20-GHz pulse train, with a pulse-width reduced to 3.2 ps from 5.6 ps. Repeating the experiment with graphene layers instead of charcoal, and detuning the cavity frequency accordingly, yielded an output pulse train of 50 GHz with a pulse train of 2.7 ps. Numerical simulations determine the effects of varying the various saturable absorption parameters, namely saturation intensity and the saturable and non-saturable absorption components of the charcoal nanoparticles. The minimum pulse-widths obtained from the simulations agree with the experiments for the same parameters.

II. Experimental Setup

To introduce charcoal nanoparticles as saturable absorbers in the fiber ring laser cavity, the method of imprinting-exfoliation-wiping process is used [19]. In the beginning, pencil nibs are ground finely, and the resulting powdered charcoal nanoparticles are brushed onto one of the end faces of a standard single mode fiber (SMF) cable. Another SMF end face is connected to this end face using a patch-cord connector which results in a sandwich of charcoal nanoparticles between the two fiber ends. They are then separated, which results in an imprinting of charcoal on both the end faces. Repeating this process multiple times yields a more even spread of charcoal over the end faces and reduces the cluster size of the sandwiched charcoal. This reduces the absorption loss caused by self-aggregation of the charcoal nanoparticles [20]. This process is outlined in Fig. 2.

The sandwiched charcoal nanoparticles are then incorporated in the fiber laser circuit as shown in Fig. 1. The fiber ring laser setup is powered by a 980 nm diode laser. The pump laser is coupled to the whole circuit via a 980/1550 nm wavelength-division multiplexer (WDM). The gain in the ring laser comes from the 23 m long Erbium doped fiber amplifier (EDFA). The output coupler (OC) ensures that only 10% of the light in the ring is output and 90% of it is fed back into the system. To ensure a unidirectional flow and no feedback, an optical isolator is also used in the circuit. To achieve passive mode-locking, the

Ashiq Rahman, Sunil Thapa, Shunyao Fan, and Niloy K. Dutta are Department of Physics, University of Connecticut, Storrs, Connecticut 06269, USA (e-mail: ashiq.rahman@uconn.edu).

patch-cord sandwiched charcoal nanoparticle is used, whereas the active mode-locking is achieved by the Mach-Zehnder Modulator (MZM). This is a $LiNbO_3$ modulator that is driven by a radio frequency of approximately 10 GHz. This driving frequency is provided by a synthesizer. The MZM used in the experiment is sensitive to polarization, hence a polarization controller is connected before the input end of the modulator. All the equipment mentioned are connected by standard 1550 nm SMF wires.

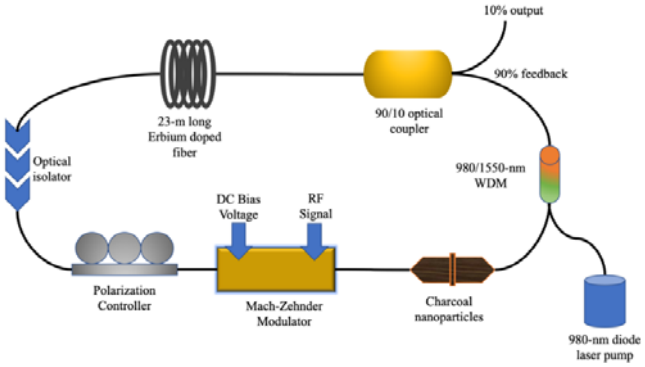

Fig. 1 Erbium doped fiber ring laser setup with charcoal nanoparticles in the cavity used as saturable absorber (WDM – Wavelength Division Multiplexer); a 980 nm laser is the pump laser needed to produce gain in the Er doped fiber

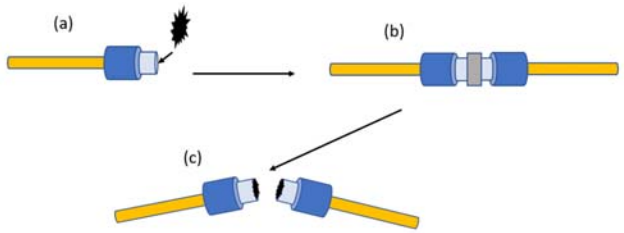

Fig. 2 Schematic of the imprinting-exfoliation-wiping process. (a) Charcoal brushed on fiber end face (b) patch cord connecting another fiber (c) process repeated to achieve required charcoal amount

III. Active and Passive Mode-Locking

A. Active Mode-Locking

The active mode-locking in this experiment is achieved using the MZM, driven by a synthesizer, as mentioned in the previous section. Carefully adjusting the polarization controllers and the output RF-frequency from the synthesizer results in just the perfect conditions necessary to obtain this phenomenon. When the modulation frequency of the laser cavity f_m satisfies the condition $f_m = (n + 1/p)\, f_c$ the laser pulses that are output from the ring laser cavity are p times the modulation frequency f_m. Here, n and p are integers, and f_c is the cavity mode sepration ($f_c = c/nL$, where c is the speed of light in vacuum, n is the average index of the fiber loop and L is the length of fiber loop). For $n = 1.5, c = 3 \times 10^8$ m/s and $L = 50$ m, the quantity $f_c = 4$ MHz. Thus, for $f_m = 10$ GHz, the quantity $n = 2500$. The deliberate detuning of f_c to an amount f_c/p from nf_c causes the laser to circulate around the ring cavity p times more before it can finally come out as pulses, hence, the output pulses have frequency that is a factor p higher. This process is called RHML, which is the active mode-locking scheme in the experiment.

B. Saturable Absorption

The saturable absorption is achieved by using the charcoal nanoparticles in the laser cavity. Charcoal nanoparticles constitute the same material as that of graphite nanoparticles, except for a few impurities and irregularities in the graphene layers, as is seen from the x-ray diffraction (XRD) spectrum. Comparing the XRD for the two types of nanoparticles, it is found that the lattice orientation of {002} yields a peak at 26.77° and 26.54°, respectively, for charcoal and graphite [21]. The size of the charcoal nanoparticles, after imprinting-exfoliation-wiping process is 300 nm, which is a considerable reduction in size from the triturated charcoal nanoparticles of diameter 500 nm (see Fig. 3).

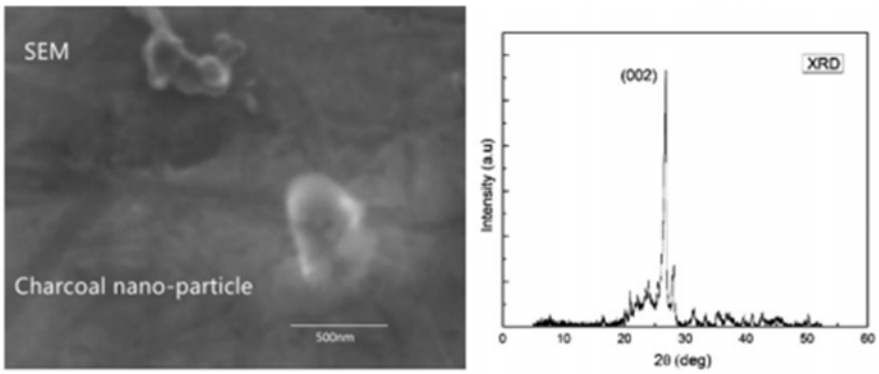

(a) (b)

Fig. 3 (a) Charcoal nanoparticles under a scanning electron microscope (SEM) and its (b) XRD spectrum showing a peak intensity at 26.77° coming from the {002} lattice orientation

Since the main composition of charcoal is graphene, the Pauli blocking effect governs its optical absorption properties [21]. Passing laser through graphene layers induces electronic transitions. When the final states are filled, the electrons are

unable to continue to make the transitions, hence the absorption of the incoming laser photons by the graphene layers ceases, and the absorption is said to be saturated. This property makes charcoal and other graphene-composed materials useful as saturable absorbers. The absorption of charcoal nanoparticle saturable absorbers is modeled using the equation [22]:

$$\alpha = \alpha_{lin} + \frac{\alpha_{non}}{1+I/I_{sat}} \quad (1)$$

As seen from the equation, the total absorption has both a linear (non-saturable) α_{lin} and a non-linear (saturable) α_{non} contribution. The non-linear term in the overall absorption is affected by the input intensity I of the laser and the intensity at which the absorption gets saturated I_{sat}.

Before running the fiber laser experiment, the modulation depth of the saturable absorber needs to be determined. This is the measure of the difference between absorptions at high and low applied intensities for a certain wavelength. A strong pulse shaping, narrower pulse-widths and reliable self-starting is achieved when the modulation depth is high. The mode-locked laser signal is passed through a variable optical attenuator (VOA) and then through the charcoal nanoparticles to determine this quantity. The same charcoal sample is then used throughout the whole experiment. For the charcoal nanoparticles used in this experiment the modulation depth is found to be 0.36, as shown in Fig. 4. As the input intensity is increased over a span of 16 $kWcm^{-2}$ to 1120 $kWcm^{-2}$, the saturable absorption decreases and the saturable transmission increases from 0.21 to 0.58, accordingly. Curve fitting shows that the linear absorption $\alpha_{lin} = 0.37$ and nonlinear absorption $\alpha_{non} = 0.48$, with an intensity of saturation at $I_{sat} = 103\ kWcm^{-2}$. This saturable absorber is then used in the main fiber ring laser circuit as was shown in Fig. 1.

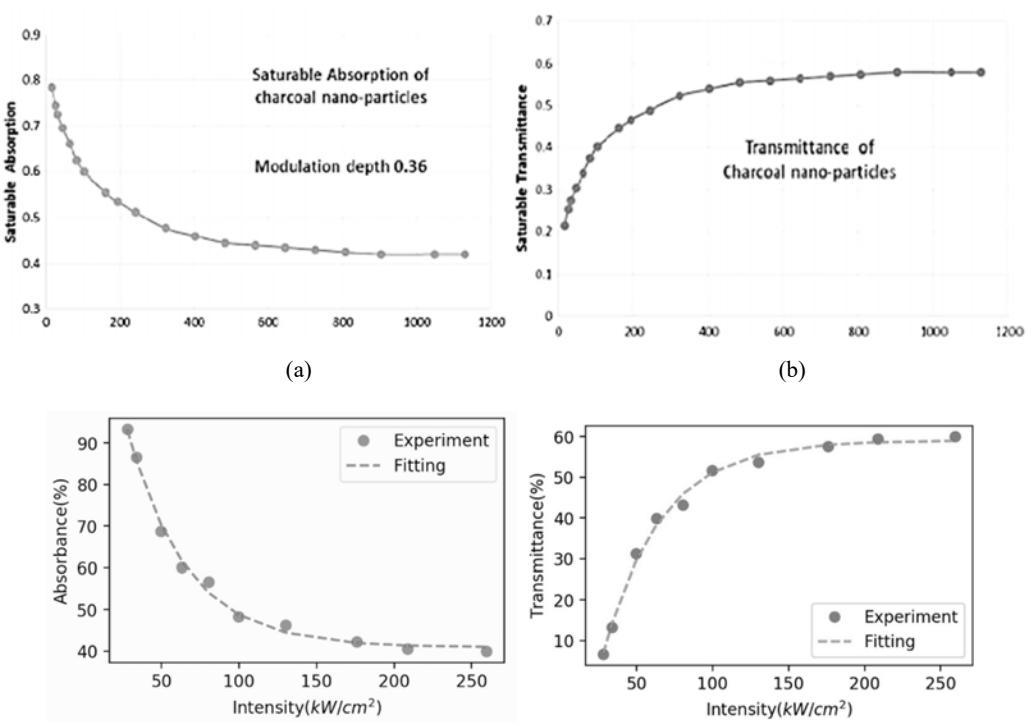

Fig. 4 (a) Saturable absorption of charcoal nanoparticles showing a modulation depth of 36%; (b) corresponding saturable transmittance of the charcoal sample; (c) Saturable absorption of graphene showing a modulation depth of 50%; (d) corresponding transmittance; both absorbers show a saturation intensity of ~100 $kWcm^{-2}$

IV. Numerical Simulation

A. Model of Pulse Propagation in Fiber Ring Laser

The propagation of laser pulses through the Erbium Doped Fiber is modeled using the Generalized Nonlinear Schrodinger Equation (GNLSE) shown in (2) [23].

$$\frac{\partial A(z,t)}{\partial z} + \frac{\alpha}{2}A(z,\tau) + \sum_{k\geq 2}\frac{i^{k-1}}{k!}\beta_k\frac{\partial^k A(z,\tau)}{\partial \tau^k} = \frac{g}{2}A(z,\tau) + \frac{g}{2\Omega_g^2}\frac{\partial^2 A(z,\tau)}{\partial \tau^2} + i\gamma|A(z,\tau)|^2A(z,\tau) \quad (2)$$

Expanding and keeping up-to the third term, the resulting equation is:

$$\frac{\partial A(z,t)}{\partial z} + \frac{i}{2}\beta_2\frac{\partial^2 A(z,\tau)}{\partial \tau^2} - \frac{1}{6}\beta_3\frac{\partial^2 A(z,\tau)}{\partial \tau^2} = \frac{g}{2}A(z,\tau) + \frac{g}{2\Omega_g^2}\frac{\partial^2 A(z,\tau)}{\partial \tau^2} + i\gamma|A(z,\tau)|^2A(z,\tau) \quad (3)$$

Now, solving (2) using the Split Step Fourier Method (SSFM) [23], the pulse propagation is found, which is characterized by the following parameters: the amplitude of the slowly varying pulse envelope $A(z,\tau)$ as a function of

propagation distance z and time-delay parameter τ, the propagation constants β_k, and the χ^3 nonlinear parameter γ. The gain g of the Erbium doped fiber in terms of the gain bandwidth Ω_g, energy of the pulse envelope E and the small signal gain g_0 is given by (4):

$$g = \frac{g_0}{(1 + E/E_{sat})} \tag{4}$$

The gain gets saturated when E is close to E_{sat}. Simulating the pulse propagation in the SMF is straightforward as in this case g is just set equal to zero.

The RHML is simulated by modeling the transmission properties of the MZM. Mathematically, the output amplitude of the MZM is given by solving [24]:

$$A(z,\tau)_{out} = A_{in}(z,\tau) \cdot \cos\left(\frac{\phi(t)}{2}\right) \quad \text{with } \phi(t) = \frac{\pi V(t)}{V_\pi} \tag{5}$$

The incoming laser is given a sinusoidal shape by the modulator. The π phase shift is achieved when the voltage between the two modulator arms is V_π. The modulator is powered by the applied voltage $V(t)$, which is itself a function of the bias voltage V_b and the amplitude of the sinusoidal RF signal $V_m \sin(\omega_m t)$ as $V(t) = V_b + V_m \sin(\omega_m t)$. The passive mode locking of the ring laser setup is modeled using the saturable absorption properties of the charcoal nanoparticles as:

$$A(z,\tau)_{out} = A_{in}(z,\tau) \cdot \left(1 - \alpha_{lin} - \frac{\alpha_{non}}{1 + I/I_{sat}}\right) \tag{6}$$

Finally, after circling through the fiber ring laser setup p times, 10% of the pulses are output and the rest of it fed back into the ring. This coupler is modeled using (7):

$$A(z,\tau)_{out} = A_{in}(z,\tau) \cdot R \tag{7}$$

Since the pulse propagates through various optical components in the laser cavity, as discussed above, various parameters representing the respective components are plugged into the simulation program. Table I summarizes the values used for all the different parameters used in solving the GNLSE and other propagation properties.

B. Effect of Various Absorption Parameters on Pulse-Width

Using the model described in the preceding section, the dependence of pulse-width on varying the saturable absorption, non-saturable absorption, and saturation intensity is studied in this section. The objective was to predict the parameter values that would result in a strong pulse shaping with the narrowest possible pulse-width. Fig. 5 shows how varying the intensity at which the absorption gets saturated would affect the pulse-width. The simulation was conducted for two values of non-saturable (linear) absorption. Both cases confirm that the pulse-width can be reduced by a factor of two at a range of $I_{sat} \sim 30 - 40\ kWcm^{-2}$. Figs. 6 and 7 show how pulse-width varies with varying linear absorption and non-linear absorption components of the saturable absorber, respectively. Both simulations were carried out for constant I_{sat} values of $40\ kWcm^{-2}$ and $100\ kWcm^{-2}$. Without using any saturable absorber, the pulse-width of a rationally harmonic mode-locked pulse is found to be 5.3 ps, whereas after incorporating the charcoal nanoparticle saturable absorber the pulse-width is compressed by up-to ~ 60%. Fig. 8 shows the effect of using charcoal saturable absorbers on the roundtrip time required to stabilize the pulses. Besides achieving a lower full-width at half-maximum (FWHM), because of a stronger pulse-shaping, the roundtrips required to stabilize the output are also less in number.

TABLE I
OPTICAL PARAMETERS USED TO MODEL THE LASER PROPAGATION IN THE FIBER LASER CAVITY

Component	Parameter	Value
Erbium	β_2	$-0.13 \times 10^{-3}\ ps^2m^{-1}$
Doped	β_3	$0.135 \times 10^{-3}\ ps^3m^{-1}$
Fiber	γ	$3.69\ W^{-1}km^{-1}$
	g_0	$10\ dBm^{-1}$
Single	β_2	$-22.1 \times 10^{-3}\ ps^2m^{-1}$
Mode	β_3	$0.171 \times 10^{-3}\ ps^3m^{-1}$
Fiber	γ	$1.20\ W^{-1}km^{-1}$
	g_0	$0\ dBm^{-1}$
Charcoal	α_{lin}	0.4
Saturable	α_{non}	0.4
Absorber	I_{sat}	$30\ kWcm^{-2}$
Coupler	R	90 %
	V_π	$6\ V$
	V_m	$6\ V$
	V_b	$3.6\ V$
Modulator	f_m	$10\ GHz$
	f_c	$2.8\ MHz$
	n	3571
	p	2 (*Charcoal expt.*)
	p	5 (*Graphene expt.*)

GNLSE is solved using the SSFM.

V. CHARCOAL EXPERIMENT RESULTS

This section presents the results of using charcoal nanoparticles as the saturable absorbers in the optical cavity. The Optical Spectrum Analyzer (OSA) output is shown in Fig. 9. Using the saturable absorber removes the noise and smoothens the output pulse. There is also an increase in bandwidth as the FWHM increases to 1.4 nm from 0.8 nm. The RF-spectrum analyzer reveals that using only the RHML yields a peak intensity at 20 GHz frequency with some super-mode noise (see Fig. 10). Like the OSA spectrum, RF spectrum shows a removal of super-mode noise and a stronger pulse shaping by the charcoal saturable absorbers. This results in more stable output pulse in RHML [3]. Fig. 11 shows the autocorrelator trace of the pulses being shortened from 5.6 ps to 3.2 ps after incorporating the charcoal saturable absorber. As a comparison, the simulation output is also provided. A good agreement between the simulation and experimental outcome is seen.

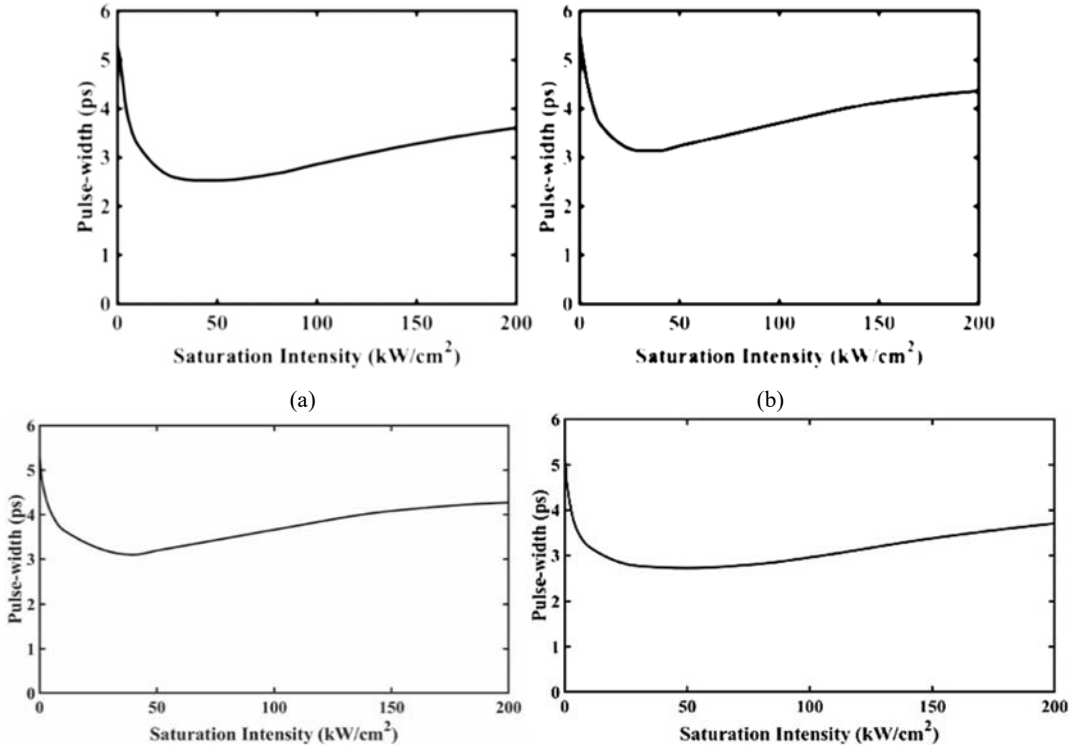

Fig. 5 Pulse-width of the mode-locked fiber laser plotted as a function of saturation intensity; the calculation was done for two different values of non-saturable absorption $\alpha_{lin} =$ 0.2 (a), (c) and 0.4 (b), (d); the saturable absorption α_{non} is 0.5 for both cases for charcoal (a), (b) and graphene (c), (d)

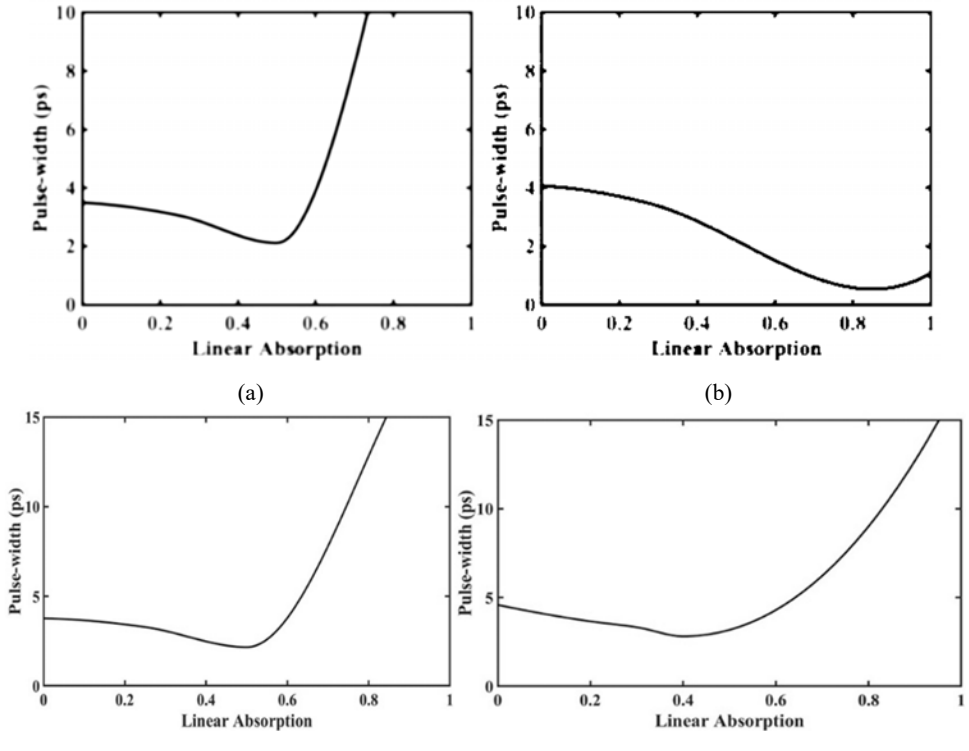

Fig. 6 Pulse-width of the mode-locked fiber laser plotted as a function of linear (non-saturable) absorption α_{lin}, for charcoal (a), (b) and graphene (c), (d), keeping the saturable part of the absorption fixed. In (a) and (c) the saturation intensity 40 $kWcm^{-2}$ and 100 $kWcm^{-2}$ in (b) and (d)

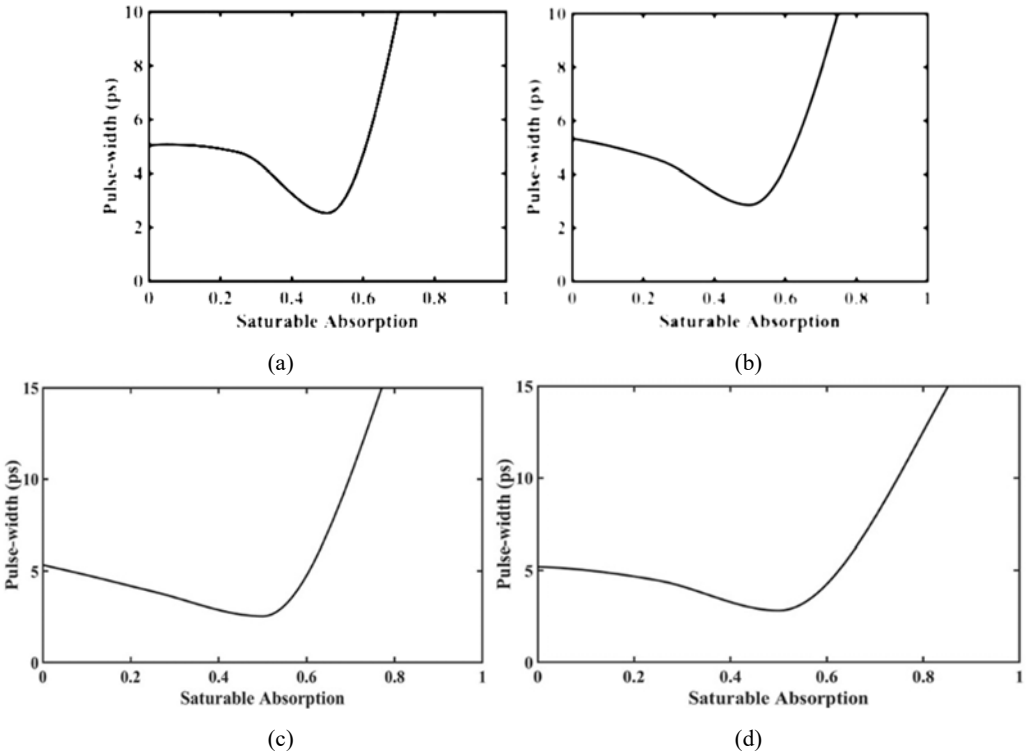

Fig. 7 Pulse-width of the mode-locked fiber laser is plotted as a function of non-linear (saturable) absorption α_{non}, for charcoal (a), (b) and graphene (c), (d), keeping the non-saturable part of the absorption fixed; saturation intensity was 40 $kWcm^{-2}$ for (a), (c), and 100 $kWcm^{-2}$ for (b), (d)

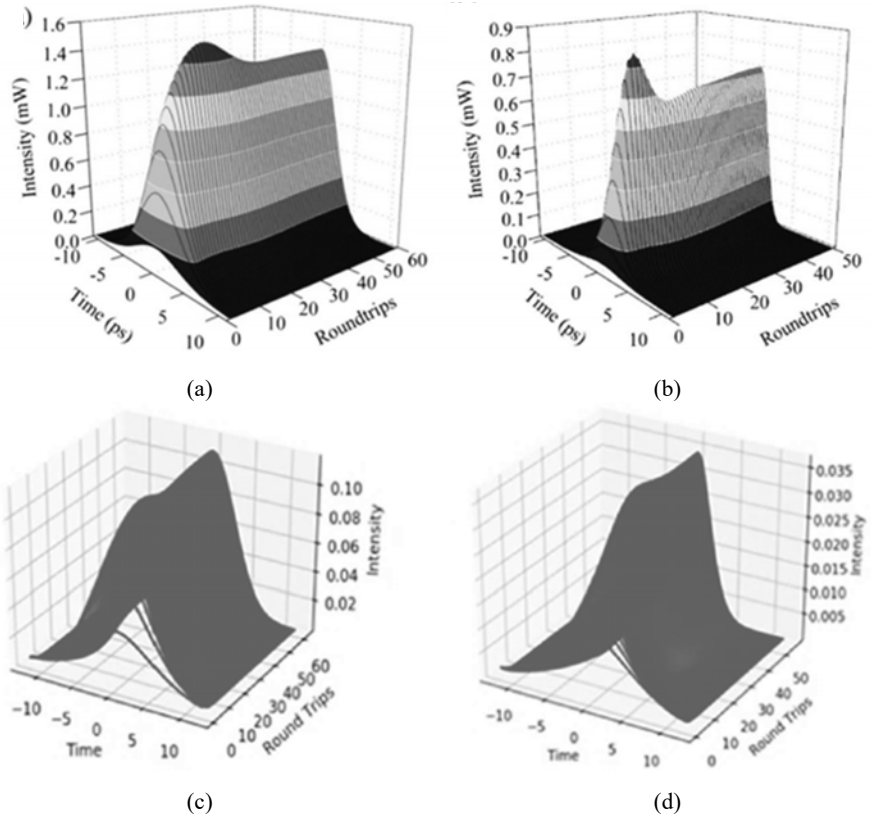

Fig. 8 Simulation of intensity vs. time vs. no. of roundtrips needed to stabilize the pulses: (a) without the saturable absorber present in the fiber ring laser cavity and (b) with saturable absorber, the output pulse-width is reduced, and the number of roundtrips required to stabilize the pulses is lesser; here, charcoal (a), (b) and graphene (c)(d) are acting as the saturable absorbers

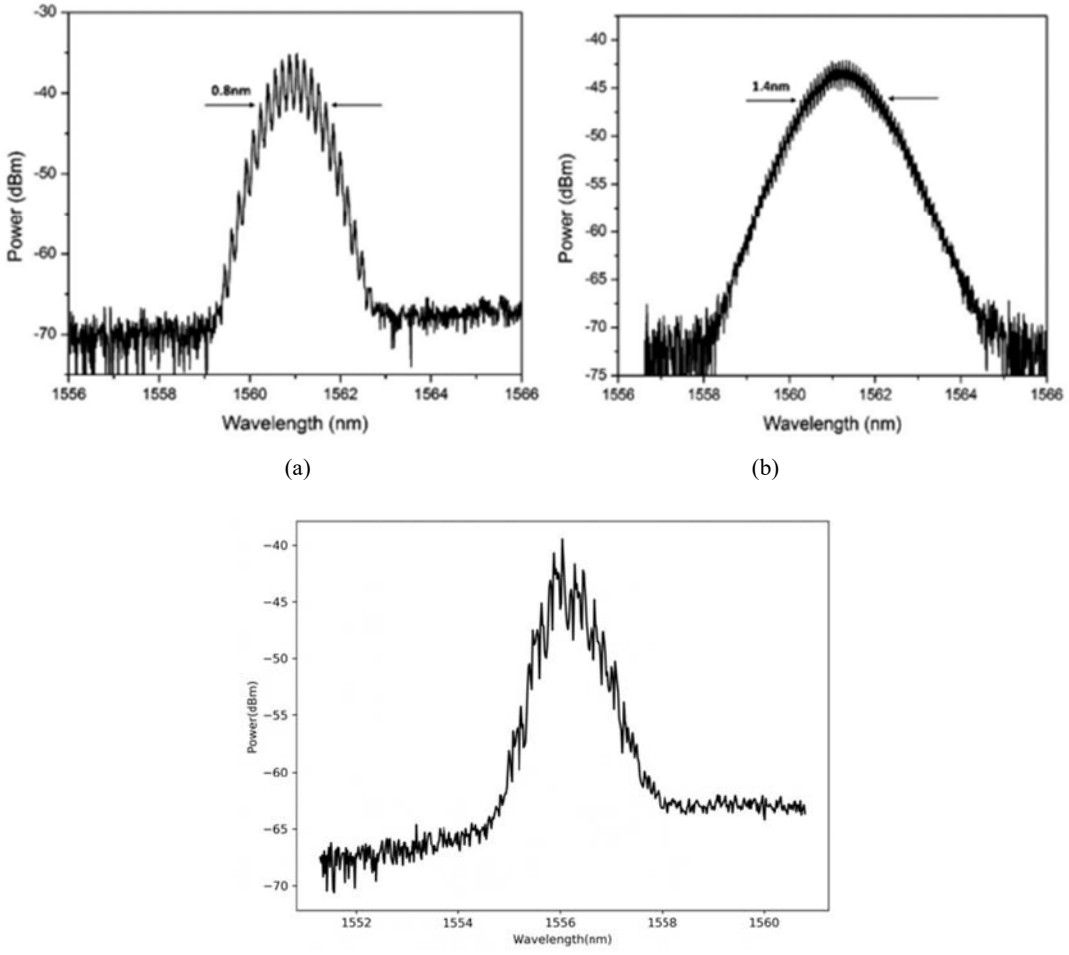

(a) (b)

(c)

Fig. 9 OSA outputs of (a) RHML only, (b) Charcoal Hybrid-ML, and (c) Graphene Hybrid-ML experiments

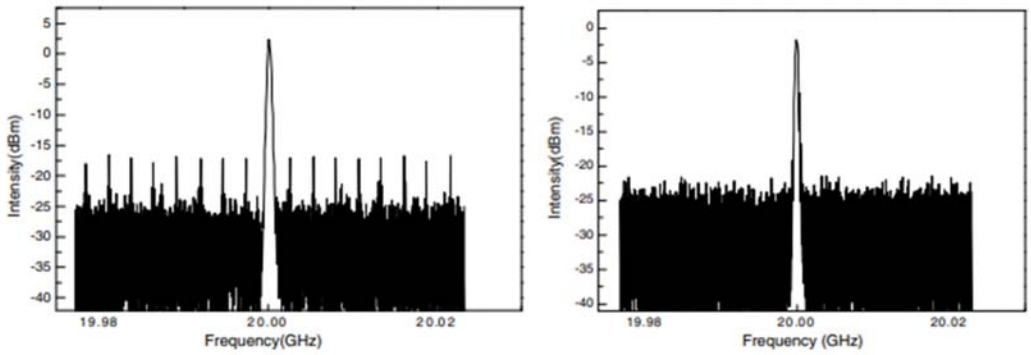

(a) (b)

Fig. 10 (a) RF spectrum of RHML obtained with and without any saturable absorber, super-mode noise is present, (b) Super-mode noise has been removed after using the charcoal saturable absorbers

VI. Conclusion

To sum up, this paper shows a method to compress the pulse-width of the output pulses from a high frequency fiber ring laser setup using RHML and charcoal nanoparticle saturable absorber. Effects of various absorbance properties, namely the linear and nonlinear absorbance components and the saturation intensity, on the pulse-width have been simulated. Triturated charcoal is shown to remove super mode noises from the RF spectrum and compress the input laser pulse-width from 5.6 ps to 3.2 ps when both the linear and non-linear absorbances are 0.4 and saturation intensity is $\sim 100\, kWcm^{-2}$. The experimental results agree with the simulation output.

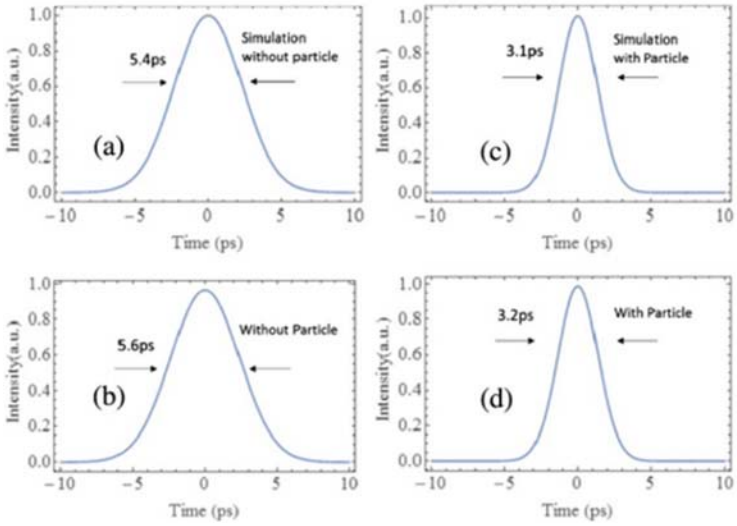

Fig. 11 Simulation of output pulses: (a) before and (b) after using charcoal nanoparticles as saturable absorbers, experimental autocorrelator output pulses: (c) before and (d) after using charcoal nanoparticles as saturable absorbers

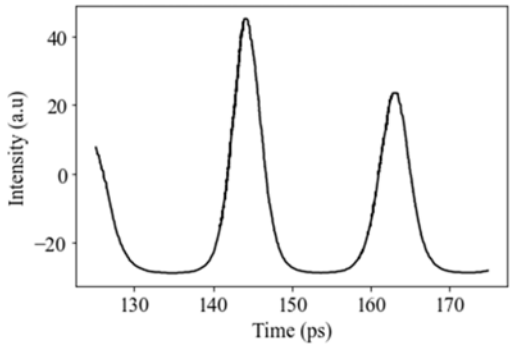

Fig. 12 Autocorrelator trace of graphene saturable absorber with output pulse train of repetition rate 50 GHz; inset shows a FWHM pulse width of 2.7 ps

DISCLOSURES

The authors declare no conflicts of interest.

REFERENCES

[1] L. Galdino et al., "Optical Fibre Capacity Optimisation via Continuous Bandwidth Amplification and Geometric Shaping," in IEEE Photonics Technology Letters, vol. 32, no. 17, pp. 1021-1024, 1 Sept.1, 2020, doi: 10.1109/LPT.2020.3007591.

[2] Z. Ahmed, and N. Onodera, "High repetition rate optical pulse generation by frequency multiplication in actively mode locked fiber ring laser," Electron. Lett. 32, 455-457 (1996).

[3] C. Wu, and N.K. Dutta, "High-repetition-rate optical pulse generation using a rational harmonic mode-locked fiber laser," IEEE J. Quantum Electron 36, 145-150 (2000).

[4] A.O. Wiberg, C.S. Bres, B.P. Kuo, J.X. Zhao, N. Alic, and S. Radic, "Pedestal-free pulse source for high data rate optical time-division multiplexing based on fiber-optical parametric process," IEEE J. Quantum Electron. 45, 1325-1330 (2009).

[5] Li, Wenbo. (2019). Different methods to achieve hybrid mode locking. Cogent Physics. 6. 10.1080/23311940.2019.1707624.

[6] Xiang Zhang, Hongyu Hu, Wenbo Li, and Niloy K. Dutta, "High-repetition-rate ultrashort pulsed fiber ring laser using hybrid mode locking," Appl. Opt. 55, 7885-7891 (2016)

[7] Q. Bao, H. Zhang, Y. Wang, Z. Ni, Y. Yan, Z.X. Shen, K.P. Loh, and D.Y. Tang, "Atomic-layer graphene as saturable absorber for ultrafast pulsed lasers," Adv. Funct. Mater.19,3077-3083 (2009).

[8] Q. Bao, H. Hang, Z. Ni, Y. Wang, L. Polavarapu, Z. Shen, Q. Xu, D. Tang, and K.P. Loh, "Monolayer Graphene as a Saturable Absorber in a Mode-Locked Laser," Nano Res 4, 297-307 (2011).

[9] G. Sobon, J. Sotor, and K.M. Abramski, "All-polarization maintain femtosecond Er-doped fiber laser mode-locked by graphene saturable absorber," Laser Phys. Lett. 9, 581-586 (2012).

[10] Wenbo Li, Hongyu Hu, Xiang Zhang, Shuai Zhao, Kan Fu, and Niloy K. Dutta, "High-speed ultrashort pulse fiber ring laser using charcoal nanoparticles," Appl. Opt. 55, 2149-2154 (2016)

[11] J.D. Zapata, D. Steinberg, L.A.M. Saito, R.E.P.de Oliveira, A.M. Cardenas, and E.A. Thoroh de Souza, "Efficient graphene saturable absorbers on D-shaped optical fiber for ultrashort pulse generation," Sci. Rep 6, 20644 (2016).

[12] Y.W. Song, S.Y. Jang, W.S. Han, M.K. Bae, "Graphene mode-lockers for fiber lasers functioned with evanescent field interaction," Applied Phys. Lett. 96, 051122-1 051122-3 (2010).

[13] Thapa, S., Rahman, A., & Dutta, N. K. (2022). Mode-locked fiber ring laser using graphene nanoparticles as saturable absorbers. International Journal of High Speed Electronics and Systems, 31 (01n04). https://doi.org/10.1142/s012915642240002x

[14] Y.H. Lin, C.Y. Yang, J.H. Liou, C.P. Yu, and G.R. Lin, "Using graphene nano-particle embedded in photonic crystal fiber for evanescent wave mode locking of fiber laser," Optics Express 21, 16763 (2013).

[15] H. Hu, X. Zhang, W. Li, and N.K. Dutta, "Hybrid Mode-Locked Fiber Ring Laser Using Graphene and Charcoal Nanoparticle as Saturable Absorbers," Proc. Of SPIE 9836, 983630 (2016).

[16] Sobon, Grzegorz & Sotor, Jaroslaw & Pasternak, Iwona & Krajewska, Aleksandra & Strupinski, Wlodek & Abramski, Krzysztof. (2013). Thulium-doped all-fiber laser mode-locked by CVD-graphene/PMMA saturable absorber. Optics express. 21. 12797-802. 10.1364/OE.21.012797.

[17] Sheng, Qiwen & Feng, Ming & Xin, Wei & Guo, Hao & Han, Tianyu & Li, Yi-Gang & Liu, Yan-Ge & Gao, Feng & Song, Feng & Liu, Zhi-bo & Tian, Jianguo. (2014). Tunable graphene saturable absorber with cross absorption modulation for mode-locking in fiber laser. Applied Physics Letters. 105. 041901-041901. 10.1063/1.4891645.

[18] Lin, Yung-Hsiang & Yang, Chun-Yu & Liin, Sheng-Fong & Lin, Gong-Ru. (2015). Triturating versatile carbon materials as saturable absorptive nano powders for ultrafast pulsating of erbium-doped fiber lasers. Optical Materials Express. 5. 10.1364/OME.5.000236.

[19] Y.H. Lin, and G.-R. Lin, "Kelly sideband variation and self-four-wave-mixing in femtosecond fiber soliton laser mode-locked by multiple exfoliated graphite nano-particles," Laser Phys. Lett. 10, 045109 (2013).

[20] Y. H. Lin, Y. C. Chi, and G.-R. Lin, "Nanoscale charcoal powder induced saturable absorption and mode-locking of a low-gain erbium-doped fiber-ring laser," Laser Phys. Lett. 10, 055105 (2013).

[21] Z. Q. Li, C. J. Lu, Z. P. Xia, Y. Zhou, and Z. Luo, "X-ray diffraction patterns of graphite and turbostratic carbon," Carbon 45, 1686– 1695

(2007).
[22] U. Keller, K. J. Weingarten, F. X. Kartner, D. Kopf, B. Braun, I. D. Jung, R. Fluck, C. Honninger, N. Matuschek, and J. Aus der Au, "Semiconductor saturable absorber mirrors (SESAM's) for femtosecond to nanosecond pulse generation in solid-state lasers," IEEE J. Sel. Top. Quantum Electron. 2, 435–453 (1996).
[23] G. P. Agrawal, Nonlinear Fiber Optics, 4th ed. (Elsevier, 2007).
[24] H. M. Chen, "A study of high repetition rate pulse generation and all-optical add/drop multiplexing," Ph.D. dissertation (University of Connecticut, 2002), Chap. 4, pp. 68.